PHYSICAL REVIEW B **92**, 085144 (2015)

Random Coulomb antiferromagnets: From diluted spin liquids to Euclidean random matrices

J. Rehn,[1] Arnab Sen,[1,2,*] A. Andreanov,[1] Kedar Damle,[3] R. Moessner,[1] and A. Scardicchio[4,5]

[1]*Max-Planck-Institut für Physik komplexer Systeme, 01187 Dresden, Germany*

[2]*Department of Theoretical Physics, Indian Association for the Cultivation of Science, Kolkata 700032, India*

[3]*Department of Theoretical Physics, Tata Institute of Fundamental Research, Mumbai 400 005, India*

[4]*Abdus Salam ICTP, Strada Costiera 11, I-34151 Trieste, Italy*

[5]*INFN, Sezione di Trieste, I-34151 Trieste, Italy*

(Received 12 May 2015; published 25 August 2015)

We study a disordered classical Heisenberg magnet with uniformly antiferromagnetic interactions which are frustrated on account of their long-range Coulomb form, i.e., $J(r) \sim -A \ln r$ in $d = 2$ and $J(r) \sim A/r$ in $d = 3$. This arises naturally as the $T \to 0$ limit of the emergent interactions between vacancy-induced degrees of freedom in a class of diluted Coulomb spin liquids (including the classical Heisenberg antiferromagnets in checkerboard, SCGO, and pyrochlore lattices) and presents a novel variant of a disordered long-range spin Hamiltonian. Using detailed analytical and numerical studies we establish that this model exhibits a very broad paramagnetic regime that extends to very large values of A in both $d = 2$ and $d = 3$. In $d = 2$, using the lattice-Green-function-based finite-size regularization of the Coulomb potential (which corresponds naturally to the underlying low-temperature limit of the emergent interactions between orphans), we find evidence that freezing into a glassy state occurs only in the limit of strong coupling, $A = \infty$, while no such transition seems to exist in $d = 3$. We also demonstrate the presence and importance of screening for such a magnet. We analyze the spectrum of the Euclidean random matrices describing a Gaussian version of this problem and identify a corresponding quantum mechanical scattering problem.

DOI: 10.1103/PhysRevB.92.085144 PACS number(s): 75.10.Jm, 05.30.Jp, 71.27.+a

I. INTRODUCTION

The appearance of novel magnetic phases [1–3] generally contains as one ingredient the ability of the system to avoid conventional (semi-)classical ordering. In this connection, the role of several factors has been extensively explored. These include low dimensionality and the resulting enhancement of the effects of quantum and entropic fluctuations, geometrical frustration, whereby the leading antiferromagnetic interactions compete with each other in lattices such as the kagome and pyrochlore lattice, and the presence of quenched disorder, which disrupts any residual tendency to conventional long-range order. Each of these has given rise to research efforts spanning decades of work.

Here, we study a model with a new combination of some of these ingredients. The focus of our study is a disordered classical Heisenberg magnet with antiferromagnetic interactions which are frustrated on account of their long-range Coulomb form at long distances, i.e., $J(r) \sim -A \ln(r/\mathcal{L})$ in $d = 2$ (where $\mathcal{L}$ is a length scale of the order of the system size) and $J(r) \sim A/r$ in $d = 3$. This Coulomb form of the Heisenberg couplings arises naturally as the $T \to 0$ limit of the emergent entropic exchange interactions [4] between vacancy-induced "orphan" degrees of freedom [5–8] in diluted Coulomb spin liquids and presents a novel variant of a disordered long-range spin Hamiltonian with connections to Euclidean random matrices. The coupling constant A is determined in any given system by the microscopic details of the underlying Coulomb spin liquid, while the spin degrees of freedom in the model we study are related to the physical orphan of the underlying diluted magnet. Our focus here is on studying the range of behaviors possible in the $T \to 0$ limit by mapping out the phase diagram of our Coulomb antiferomagnet as a function of A. Frustration arises naturally in the model under consideration, as *any* triplet of spins are mutually coupled antiferromagnetically but without the randomness in sign of, say, the Sherrington-Kirkpatrick model [9]. Also, unlike the latter case, the interactions are long-ranged but not independent of distance.

Our motivations for studying it include having been led to this model in a previous investigation [10] of diluted frustrated magnets exhibiting a Coulomb spin liquid at low temperatures. The model is, in this sense, natural, appearing as the zero-temperature limit of a disordered frustrated magnet. The corresponding experiments are on the material known as SCGO, which triggered the interest in what we now call highly frustated magnetism in the late 80s [11]. Its behavior at very low temperatures is still not very well understood, e.g., the observed glassiness even at very low impurity densities (as low as 2% of the Cr sites occupied by nonmagnetic Ga atoms in SCGO [12–14]), which appears to involve only the freezing of a fraction of its degrees of freedom. Similar experiments have recently been conducted on the three-dimensional spinel compound ZCGO [15]. We return to this point in Sec. VII B. While exhibiting a classical Coulomb spin-liquid regime, the disorder in this system leads to the emergence of new, fractionalized, degrees of freedom, the so-called orphans [5,6], which interact via an effective entropic long-range interaction mediated by their host spin liquid [4].

We believe that, as such, it can be of interest as a generic instance of the interplay of strong interactions and disorder in magnetism [16,17]. In particular, it develops the strand of thought of how disorder in a topological system characterized by an emergent gauge field can nucleate gauge-charged defects, with the pristine bulk mediating an effective

*jorgerehn@pks.mpg.de

interaction between them. Long-range Coulomb interactions like the one studied here are thus as natural as the algebraically decaying RKKY interactions in metallic spin glasses.

Our central results are the following. First, we use the results of previous work [4] to work out in detail the key features of this $T \to 0$ limit and demonstrate that this limit is characterized by a single coupling constant A, which is, in principle, determined by the geometry of the underlying spin liquid. Second, our extensive Monte Carlo (MC) simulations for $d = 2$ reveal no sign of any freezing or ordering transition up to very high coupling strengths. At the same time, within a self-consistent Gaussian approximation, we find that such a transition does appear at infinite coupling in $d = 2$ but not in $d = 3$. This transition is very tenuous, in that it is replaced by a more conventional ordering transition in a finite system depending on the choice of how to regularize this long-range interaction in a finite lattice: the finite-size lattice regularization that is most natural from the point of view of the $T \to 0$ limit of the underlying diluted magnet gives rise to freezing into a glassy state at $A^{-1} = 0$, while other regularizations replace this glassy state with a conventional ordering pattern. The Coulomb antiferromagnet therefore remains highly susceptible to perturbations, just like many other frustrated magnets [1].

We also study the spectrum of the interaction matrix of this random Coulomb antiferromagnet, which provides an instance of a Euclidean random matrix (ERM) [18,19], in that its entries are obtained as a distance function between randomly chosen location vectors. We find two qualitatively distinct regimes. On one hand, at low energies in the low-density limit, eigenfunctions are localized, with the lowest energy states as pairs of neighboring spins the probability distribution of which we compute. Beyond this extreme low-density limit, more complex lattice animals appear in this regime. On the other hand, at high energies, the modes correspond to long-wavelength charge density variations with superextensive energy. In between, we find no clear signature of a well-defined mobility edge in this Coulomb system.

Another interesting aspect of the uniformly antiferromagnetic interactions is that they permit a variant of screening to appear in this Coulomb magnet, which has no correspondence with other long-range magnets such as the Sherrington-Kirkpatrick model. Our analysis of this screening further leads us to an identification of the correlations of the random Coulomb antiferromagnet with the properties of the zero-energy eigenstate of a quantum particle in a box with randomly placed scatterers.

Returning to experiments, we note that the uniform magnetic susceptibility of SCGO will of course be dominated by the Curie tail ($\sim 1/T$) produced by these orphans at low temperatures. Both in $d = 2$ and in $d = 3$, the full susceptibility, when vacancies are placed at random, is that of *independent* orphans to a good approximation despite the long-ranged interaction present between them. This persists down to the lowest temperatures not only because of the screening of the interactions at finite physical temperature, but also because the size of the Coulomb coupling derived from the entropic interaction is comparatively weak. In addition, the physical orphans are related to the degrees of freedom in the Coulomb antiferromagnet via a sublattice-dependent staggering transformation, so that the *uniform* susceptibility of the physical orphans corresponds to the staggered susceptibility of the degrees of freedom of our Coulomb antiferromagnet. As a result, the uniform susceptibility remains largely unaffected by the fact that the total (vector) gauge charge of our Coulomb antiferromagnet vanishes.

The remainder of this paper is structured as follows. In Sec. II, we first provide a self-contained review of earlier work on vacancy-induced effective spins in a class of classical antiferromagnets on lattices consisting of "corner sharing units" and then build on this to provide a careful derivation of the $T \to 0$ limit of the emergent entropic interactions between orphans and use this to define our model Coulomb antiferromagnet. After outlining our analytical and numerical approaches in Sec. III, we present the results obtained in $d = 2$ and $d = 3$ (Sec. IV). Section V contains the analysis of the problem in terms of an ERM, while the role of screening and the connection to a scattering problem are discussed in Sec. VI. We conclude with a discussion of these results and relegate sundry details (such as discussion of the fully occupied lattice and the ordered state seeded by a certain finite-lattice regularization of the two-dimensional Coulomb interaction) to the appendixes.

II. THE RANDOM COULOMB ANTIFERROMAGNETIC HAMILTONIAN

We thus study a classical Heisenberg model,

$$H = \frac{1}{2} \sum_{i,j} J_{ij} \vec{n}_i \cdot \vec{n}_j, \tag{1}$$

where J_{ij} takes on a Coulomb form,

$$J_{ij} = -A \log(r_{ij}/\mathcal{L}) \quad (d = 2) \tag{2}$$

$$= A/r_{ij} \quad (d = 3). \tag{3}$$

This form with $\mathcal{L}$ larger than any r_{ij} has the property that the interactions are uniformly antiferromagnetic as well as long-ranged.

We need to supplement this by defining the degrees of freedom, unit vectors $\vec{n}_i$, appearing in Eq. (1). We concentrate on the case where their locations, denoted i, are chosen randomly on a square (cubic) lattice in $d = 2$ ($d = 3$), at a dimensionless density of x spins per lattice site.

For long-range interactions like this Coulomb interaction, choices about boundary conditions or ensemble constraints can be considerably less innocuous than for short-range systems. In order to illustrate this, and to make natural choices for these items, as well as for motivation of our study, we next discuss the derivation of a random Coulomb antiferromagnet as an effective Hamiltonian of a diluted Coulomb spin liquid.

A. Orphan spins and their interactions in diluted Heisenberg antiferromagnets

We thus begin by providing a self-contained review of earlier work on vacancy-induced effective spins in a class of classical frustrated antiferromagnets on lattices consisting of "corner-sharing units." The centers of these in turn define a so-called premedial lattice, which is bipartite in practically all

instances of the popularly studied classical Heisenberg spin liquids [8]. A simple model of nearest-neighbor antiferromagnetically interacting spins on such lattices can be written as

$$H = \frac{J}{2}\sum_{i,j}\vec{S}_i\cdot\vec{S}_j = \frac{J}{2}\sum_{\boxtimes}\left(\sum_{\vec{l}\in\boxtimes}\vec{S}_{\vec{l}}\right)^2, \tag{4}$$

where the summation in the alternate form of the Hamiltonian is carried over the cornersharing simplices $\boxtimes$, which might be tetrahedra, as, e.g., in a pyrochlore lattice, triangles in a Kagome lattice, or a combination of both, as in the case of SCGO, and the spins of the frustrated magnet are now labeled $\vec{l}$, the links of the bipartite premedial graph (whose sites correspond to the centers of the simplices $\boxtimes$ of the original lattic and links $\vec{l}$ correspond to sites of the original lattice). When written in this form, it is clear that ground-states are characterized by the constraints:

$$\sum_{\vec{l}\in\boxtimes}\vec{S}_{\vec{l}} = 0, \forall\,\boxtimes\,. \tag{5}$$

These local constraints lead to an effective description in terms of a theory of emergent electric fields that obey a Gauss law. To see this, we define electric fields $\mathbf{E}^{\alpha}_{\vec{l}} = \epsilon_{\vec{l}}S^{\alpha}_{\vec{l}}$ on links $\vec{l}$, where $\epsilon_{\vec{l}}$ is a spatial unit vector that points from the A to the B sublattice of the premedial lattice end of this link. The ground-state condition then translates to the statement that the lattice divergence of this electric field vanishes at each site $\boxtimes$ for each α. The key idea of this effective description is that the coarse-grained (entropic) free energy density depends quadratically on the local electric field, and deviations from the vanishing divergence condition amount to the appearance of vector Coulomb charges [4]. These emergent gauge charges are defined for each lattice point $\boxtimes$ of the bipartite premedial lattice,

$$\vec{Q}_{\boxtimes} = \eta(\boxtimes)\sum_{\vec{l}\in\boxtimes}\vec{S}_{\vec{l}}, \tag{6}$$

and the staggering factor, $\eta(\boxtimes) = +1$, if $\boxtimes$ is an A-sublattice site in the premedial graph, and -1 otherwise. Since each microscopic spin contributes with opposite signs to the vector charge on two neighboring simplices, the total gauge charge of a system without boundaries must vanish in every configuration of the system,

$$\sum_{\boxtimes}\vec{Q}_{\boxtimes} = 0. \tag{7}$$

This very natural condition—akin to the charge neutrality of the full universe and, in our case, unavoidable due to the microscopic origin of the emergent gauge charge—is explicitly imposed in our MC simulations of the system.

The mapping of the pure system to an emerging gauge field theory at low temperatures makes clear that generalized "vector charges," $\vec{Q}_{\boxtimes}$, are generated thermally as a consequence of the violation of the ground-state constraints. The constraint, Eq. (5), is also unavoidably violated in the presence of nonmagnetic impurities (Fig. 1) whenever all but one spin of a given simplex are substituted for by vacancies (simplices containing at least two spins can in general satisfy the zero-total-spin condition, and such simplices do not host a vector charge in the $T \to 0$ limit). Indeed, when all spins but one in a simplex are replaced by vacancies, the result is a paramagnetic Curie-like response [4,6,10], which dominates the susceptibility response at low temperatures. The lone spins on these defective simplices, which serve as the epicenter of this paramagnetic response, were baptized *orphans* [5] in the first studies of this effect.

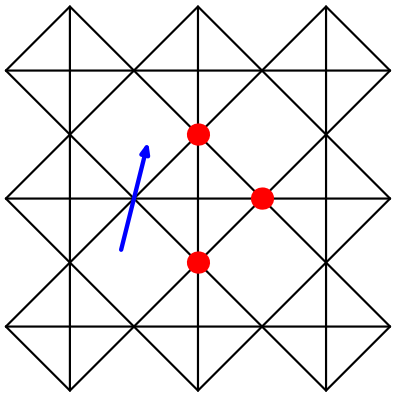

FIG. 1. (Color online) Illustration of the orphan spin arising from the introduction of nonmagnetic impurities [(red) circles] on the checkerboard lattice. Its effective moment is half that of a free spin.

The field theory developed in Refs. [4] and [10] extends the self-consistent Gaussian approximation (SCGA) [20], a theory successful in describing low-temperature correlations in undiluted systems, to incorporate the effects of dilution and study the physics of these orphans at nonzero temperature in a manner that treats entropic effects on an equal footing with energetic considerations. In its original form the SCGA replaces the hard constraint on the spin norm, $\vec{S}_i^2 = S^2$, with the relaxed *soft spin* condition on their thermal average, $\langle\vec{S}_i^2\rangle = S^2$. The key insight in Refs. [4] and [10], which led to the detailed analytical understanding summarized below, was the following: While it is sufficient to treat in this self-consistent Gaussian manner all spins other than the lone orphan in a simplex in which all but one spin has been replaced by vacancies, this is much too crude an approximation for the orphan itself, which must be treated without approximation as a hard spin obeying $\vec{S}^2_{\text{orphan}} = S^2$. Remarkably, the resulting hybrid field theory continues to be analytically tractable when the number of orphans is small [4,10]. With just one orphan present in a sample with an external magnetic field of strength B along the z axis, the theory predicts that this orphan sees a magnetic field $B/2$, with the other half of the external field screened out by the coupling to the bulk spin liquid. The resulting polarization of the orphan serves as a source for an oscillating texture that spreads through the bulk. The net spin carried by the texture cancels half the spin polarization of the orphan, resulting in an impurity susceptibility corresponding to a classical spin $S/2$. With more than one orphan present, the spin textures seeded by each orphan mediate an effective entropic interaction between each pair of orphans.

The effective action for a pair of orphans is predicted in this manner to have the form

$$-\beta J_{\text{eff}}(\vec{r},T)\vec{n}_1\cdot\vec{n}_2, \tag{8}$$

where $\vec{n}$ are unit vectors corresponding to the directions of the orphans in a given configuration. The exchange coupling has a particularly simple form in the large separation limit

$$\beta J_{\text{eff}} \approx -\eta(\vec{r}_1)\eta(\vec{r}_2)\frac{\langle \vec{Q}_{\boxtimes}(\vec{r}_1)\cdot\vec{Q}_{\boxtimes}(\vec{r}_2)\rangle}{\langle \vec{Q}_{\boxtimes}\cdot\vec{Q}_{\boxtimes}\rangle^2}, \tag{9}$$

which involves only "charge-charge" correlations *calculated in the pure system*:

$$\langle \vec{Q}_{\boxtimes}(\vec{r}_1)\cdot\vec{Q}_{\boxtimes}(\vec{r}_2)\rangle \sim -T^2T^{d/2-1} \times \int^{\Lambda/\sqrt{T}} d^dq \frac{\exp(i\vec{q}\cdot(\vec{r}_1-\vec{r}_2))}{\Delta_c q^2+\kappa}. \tag{10}$$

The denominator of Eq. (9) behaves at low temperatures as $\langle \vec{Q}_{\boxtimes}\cdot\vec{Q}_{\boxtimes}\rangle = T/J$ from equipartition.

For orphans in $d = 2$, one finds

$$J_{\text{eff}}(\vec{r}_1-\vec{r}_2,T) = \eta(\vec{r}_1)\eta(\vec{r}_2)T\mathcal{J}(|\vec{r}_1-\vec{r}_2|/\xi_{\text{ent}}), \tag{11}$$

with an entropic screening length $\xi_{\text{ent}} = 1/\kappa \sim 1/\sqrt{T}$ separating two regimes for $\mathcal{J}(\kappa r)$: for $\kappa r \ll 1$ a logarithmic one, $\mathcal{J}(\kappa r) \sim -\log(\kappa r)$; and for $\kappa r \gg 1$ a screened regime, $\mathcal{J}(\kappa r) \sim \frac{1}{\sqrt{\kappa r}}\exp(-\kappa r)$. Analogously, in $d = 3$,

$$J_{\text{eff}}(\vec{r}_1-\vec{r}_2,T) = \eta(\vec{r}_1)\eta(\vec{r}_2)T^{3/2}\mathcal{K}(|\vec{r}_1-\vec{r}_2|/\xi_{\text{ent}}), \tag{12}$$

and the entropic screening length $\xi_{\text{ent}} = 1/\kappa \sim 1/\sqrt{T}$ separates two regimes, algebraic $\mathcal{K}(r) \sim -1/r$ and screened $\mathcal{K}(r) \sim \exp(-\kappa r)$.

In the physical system, at any nonzero temperature, this is thus a "short-ranged" interaction on account of the finite screening length, which, however, diverges as $1/\sqrt{T}$. In this article, we are interested in the limit of $T = 0$, where the interaction takes on the novel—for magnetic systems—long-range Coulomb form.

B. Model Hamiltonian

In the limit of $T \to 0$, we are thus led by these considerations to Coulomb interactions between the vector orphans, which we study in detail here. For simplicity, we consider unit-vector spins $\vec{n}$ at random locations in a periodic hypercubic lattice of linear size L with occupancy probability x, corresponding to an underlying spin liquid on the checkerboard and "octochlore" lattices of corner-sharing units involving 2^d spins in d dimensions.

In what follows, we get rid of the sublattice factors that affect the sign of the effective interaction by inverting all unit vectors placed on the B sublattice. In other words, we identify $S\vec{n}_i$ with $\eta_i\vec{S}_{\text{orphan},i}$, where $\vec{S}_{\text{orphan},i}$ is the orphan on the simplex labeled i in the underlying diluted frustrated magnet.

This gives us a "random Coulomb antiferromagnet" in which unit-vector spins interact with an exchange coupling that is always antiferromagnetic but of a long-range Coulomb form at large distances. For a classical system, this transformation is innocuous, but note that natural observables cease to be so under this mapping; e.g., the orphan contribution to the uniform susceptibility of the underlying diluted magnet is now given by the staggered susceptibility of our Coulomb antiferromagnet.

As is usual for entropic interactions in the limit of $T \to 0$, the strength of their coupling, A, is fixed by the microscopics of the model from which they have emerged. In this work, we are interested in exploring the generic behavior of such models—in particular, identifying possible phases—and thus allow the coupling A to be variable. For completeness, we mention that $A = \frac{1}{4\pi}$ for the checkerboard lattice.

This therefore leads to the form of H at the beginning of this section, Eq. (1). To make Eq. (2) dimensionally unambiguous we write

$$J_{ij} = -A\log(r_{ij}/\mathcal{L}) \quad (d = 2),$$

with $\mathcal{L}$ conveniently set to a value of the order of the system size L so that $J_{ij} > 0$ always. In the above language, with sublattice factors η absorbed into the definitions of $\vec{n}_i$, the zero-gauge-charge constraint imposed by the microscopic origin of this effective model now translates to the constraint that $\sum_i \vec{n}_i = 0$ in every allowed configuration of our Coulomb antiferromagnet. This constraint in fact can also be imposed by adding an infinitely strong interaction acting equally between all spins. This equivalence renders the detailed choice of $\mathcal{L}$ immaterial.

We note an interesting scale invariance of this model in the limit of low densities of spins. This scale invariance is inherited from that of the logarithmic function under scaling transformations, $J(\kappa r) = \log(\kappa) + J(r)$, together with net charge neutrality, Eq. (7),

$$\sum_i \vec{n}_i = 0, \tag{13}$$

implying that the extra term $\log(\kappa)$ gives a temperature-independent contribution to the action determined by $1/2\sum_{i\neq j}\vec{n}_i\cdot\vec{n}_j = -N/2$. The partition function thus only picks up a constant factor:

$$Z' = e^{-\beta\sum_{i,j}J(\kappa r_{ij})\vec{n}_i\cdot\vec{n}_j} = e^{\beta\log(\kappa)N/2}Z. \tag{14}$$

This also means that, rather unusually, in the continuum limit $x \to 0$ the partition function is a scaling function depending on the randomly chosen orphan locations only scaled by their mean separation. Lattice discretization effects at finite x break this equivalence. The scaling transformation for the model in three dimensions gives $J(\kappa r) = J(r)/\kappa$, which implies, for the partition function, a rescaling of β:

$$Z'(\beta) = e^{-\beta\sum_{i,j}J(\kappa r_{ij})\vec{n}_i\cdot\vec{n}_j} = Z(\beta/\kappa). \tag{15}$$

For Coulomb interactions in a finite-size system, various choices of the interaction yield the same long-distance form in the limit $L \to \infty$. The most natural form from the point of view of the effective field theory predictions for emergent interactions between orphans is the Fourier transform of the inverse of the lattice Laplacian, $d - \sum_{i=1}^d \cos k_i$:

$$J(r_{ij}) = \frac{\pi}{L^2}\sum_{\vec{q}}\frac{e^{i\vec{k}\cdot\vec{r}_{ij}}}{d-\sum_{i=1}^d\cos k_i}. \tag{16}$$

We call this the lattice Green function (LGF), and our most detailed studies are carried out using this form of the interaction.

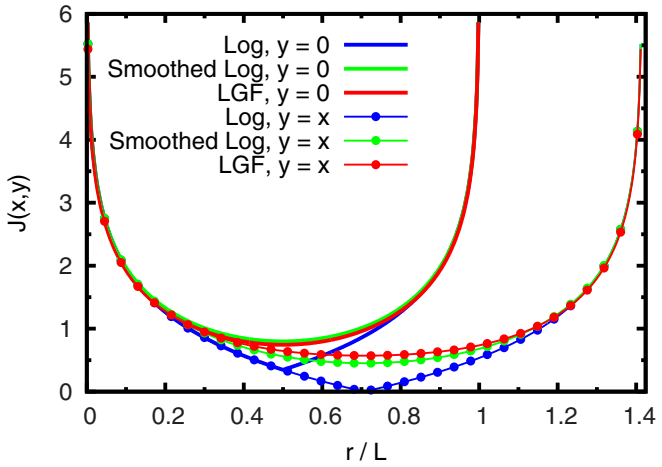

FIG. 2. (Color online) $J(x,y)$ used in the simulations in $d = 2$.

Alternatively, one can work directly with the Coulomb form, e.g., for $d = 2$,

$$J(r_{ij}) = -\log\left(\frac{r_{ij}}{\mathcal{L}}\right), \tag{17}$$

with $\mathcal{L} = L/\sqrt{2}$. This form agrees with the LGF interactions at short distances (see Fig. 2).

The issue of how to impose the boundary conditions, and therefore how to compute r_{ij}, turns out to make a large difference in the results for a finite system, as we shall see. The choices of either

$$r_{ij} = |\vec{r}_i - \vec{r}_j| = \sqrt{\tilde{x}_{ij}^2 + \tilde{y}_{ij}^2}, \tag{18}$$

with $\tilde{x}_{ij} = \min(|x_i - x_j|, L - |x_i - x_j|)$, or

$$r_{ij} = \frac{L}{\pi}\sqrt{\sin^2\left(\frac{\pi(x_i - x_j)}{L}\right) + \sin^2\left(\frac{\pi(y_i - y_j)}{L}\right)} \tag{19}$$

result in different behaviors for the system, which are explained in more detail in Sec. IV. We refer to these choices as periodized, and smoothed, logarithms, respectively. The latter is very close to the LGF, while the former maintains a finite difference from it at the periodic boundary, where it is not differentiable for any L (Fig. 2). It is easily seen why this finite difference is independent of L, if one compares the smoothed log to the periodized log, approximately equivalent to comparing the LGF with the log. Looking, e.g., at the midpoint of one edge ($x_{ij} = L/2$, $y_{ij} = 0$), one finds

$$(J_L^{\mathrm{LGF}} - J_L^{\log})(L/2,0) \approx \log(\pi/2), \tag{20}$$

where the subscript L emphasizes that we are looking at the respective forms of the interactions in a finite system of size L. Note, again, that adding a constant to the interaction (in $d = 2$), e.g., by changing the denominator of Eq. (17), leaves the interaction unchanged due to the global charge neutrality constraint.

III. METHODS

The analysis of spin systems with the potential for glassy phases is a delicate endeavor, as equilibration of large systems is elusive. The existence and determination of a transition temperature are usually a controversial issue [21,22]. Since our system has long-ranged interactions, boundary effects can cause yet more trouble. This is why we combine analytical with numerical methods, as well as mappings to other problems which have received attention in a different context previously.

Numerically, we study the behavior of this model through MC simulations and analytically in the self-consistent Gaussian ("large-m"; also denoted the LM approach in the following [23–25]) approximation, where the parameter A mimics an inverse temperature. Our MC simulations directly impose the constraint, Eq. (7). For this we initialize the system in a random configuration of vanishing total spin, and the update movements in the system consist of selecting an arbitrary pair of spins and rotating them around the axis determined by their vectorial sum. An MC simulation of the same system with strictly positive interactions, without this constraint on the total spin, has also been investigated, and the conclusion is that while the relaxation time increases, the system still prefers to stay close to the manifold of vanishing total spin.

The LM approach consists of considering spins with m components and letting $m \to \infty$. This is formally equivalent to the soft-spin approximation and it only gives, in principle, information about the infinite number of components limit, but this can be understood as the first term in an expansion of the $O(m)$ model. It has been very successful in the analytical study of correlations in highly frustrated spin systems [20], being able to reproduce the main features of the ongoing phenomena, such as the existence of long-range dipolar correlations at $T = 0$, characterized by the presence of "pinch points" in the structure factor [26].

The LM approach allows an analysis of the system both at finite coupling strengths $A < \infty$ and at $A = \infty$. The study of glassiness using this approach has already been undertaken in a variety of models [25,27], and we follow a similar methodology. Correlations are computed through the matrix

$$B_{ij} = J_{ij} + h_i\delta_{ij} \tag{21}$$

and are given by

$$C_{ij} = \frac{1}{m}\langle\vec{n}_i \cdot \vec{n}_j\rangle = \frac{1}{A}(B^{-1})_{ij}. \tag{22}$$

These can be computed once the Lagrange multipliers, h_i, are determined through the set of nonlinear equations:

$$C_{ii} = 1. \tag{23}$$

For comparison between the LM and the MC, we scale observables and couplings with m so that their small-coupling ("high-temperature") forms agree.

The point $A = \infty$ is treated within the LM approach by determining the (unique [23]) ground state through a *local field quench* algorithm [28]. This algorithm is based on the fact that if the number of spin components, m, is large enough (larger than $\sqrt{2N}$[23]), then a system of spins with m components is effectively equivalent to the corresponding system in the limit $m \to \infty$. The algorithm then consists of taking a system of N

spins with $m > \sqrt{2N}$ components initially randomly oriented and then iteratively aligning each spin with its local field. This procedure is expected to converge to the unique ground state, from which all the quantities of interest can be computed.

A fundamental quantity at $A = \infty$ within the LM approach is the number of zero eigenvalues, m_0, of the matrix $B_{ij} = J_{ij} + h_i\delta_{ij}$; it can be shown [23] that the ground-state spin vectors span an m_0-dimensional space. This quantity should scale with the number of particles in the system as $m_0 \sim N^{\mu}$.

The main quantity of interest in our study is the spin-glass susceptibility (square brackets here and throughout indicate the disorder average),

$$\chi_{SG}(\vec{k}) = \left[\frac{1}{N}\sum_{i,j}\langle\vec{n}_i\cdot\vec{n}_j\rangle^2\cos\vec{k}\cdot(\vec{r}_i-\vec{r}_j)\right], \tag{24}$$

obtained in the MC simulations through the overlap tensor [3],

$$Q^{\alpha,\beta}_{\vec{k}} = \frac{1}{N}\sum_i n^{\alpha}_{i,1}n^{\beta}_{i,2}e^{i\vec{k}\cdot\vec{r}_i}, \tag{25}$$

where Greek indices refer to the spin components, while the indices 1 and 2 refer to two independent replicas of a disorder realization. This might be interpreted as the overlap of a spin configuration with itself after an infinitely long time. Since the onset of glassiness can also be understood as a divergence of the equilibration time, the nonvanishing of this order parameter signalizes the transition.

The spin-glass susceptibility in terms of this tensor is

$$\chi_{\rm SG}(\vec{k}) = \left[N\sum_{\alpha,\beta}\langle|Q^{\alpha,\beta}_{\vec{k}}|^2\rangle\right]. \tag{26}$$

We follow the usual practice to determine the spin glass transition by computing a finite system correlation length associated to the susceptibility above. The Ornstein-Zernike form for correlations gives:

$$\xi_L = \frac{1}{2\sin(k_{\rm min}/2)}\left(\frac{\chi_{\rm SG}(0)}{\chi_{\rm SG}(\vec{k}_{\rm min})}-1\right)^{1/2}, \tag{27}$$

and near the transition, the finite size scaling prediction is expected to be:

$$\frac{\xi_L}{L} = X(L^{1/\nu}(1/A-1/A_c)), \tag{28}$$

while the susceptibility should follow:

$$\frac{\chi_{\rm SG}}{L^{\gamma/\nu}} = Y(L^{1/\nu}(1/A-1/A_c)), \tag{29}$$

Notice that these scaling relations only hold if there exists a crossing of finite size correlation length curves for different system sizes at an unique finite coupling strength value. The absence of such a crossing at a finite A_c indicates the absence of a phase transition. Nonetheless a phase transition at $A_c = \infty$ cannot thus be ruled out and the LM approach allows an analysis in this situation. The scaling relations predicted to hold in this case ($A_c \to \infty$) are:

$$\chi_{\rm SG} = L^{d(1-\mu)}Y(L^{1/\nu}/A), \quad \xi_L/L = X(L^{1/\nu}/A). \tag{30}$$

The exponent μ here is the one previously introduced for the scaling of the number of zero eigenvalues of the matrix B with the number of particles in the system. Furthermore, as was shown in Ref. [25], the same exponent controls the scaling of the spin glass susceptibility for the ground state configuration: $\chi_{\rm SG} \sim N^{1-\mu}$.

IV. RESULTS

A. Two dimensions

The two approaches (MC and LM) yield a broadly consistent picture for each of the interactions studied. We conduct an analysis of a possible freezing transition in the model by measuring the spin glass susceptibility and trying to identify the transition through a finite size scaling of its associated correlation length. Other observables such as the specific heat or the uniform susceptibility were also studied, though these do not indicate any of the conventional orderings.

The results from MC simulations and LM calculations are shown in Fig. 3 for a system with the LGF as the interaction for a fixed density $x = 0.10$ of particles. In each case the number of disorder realizations simulated was 200.

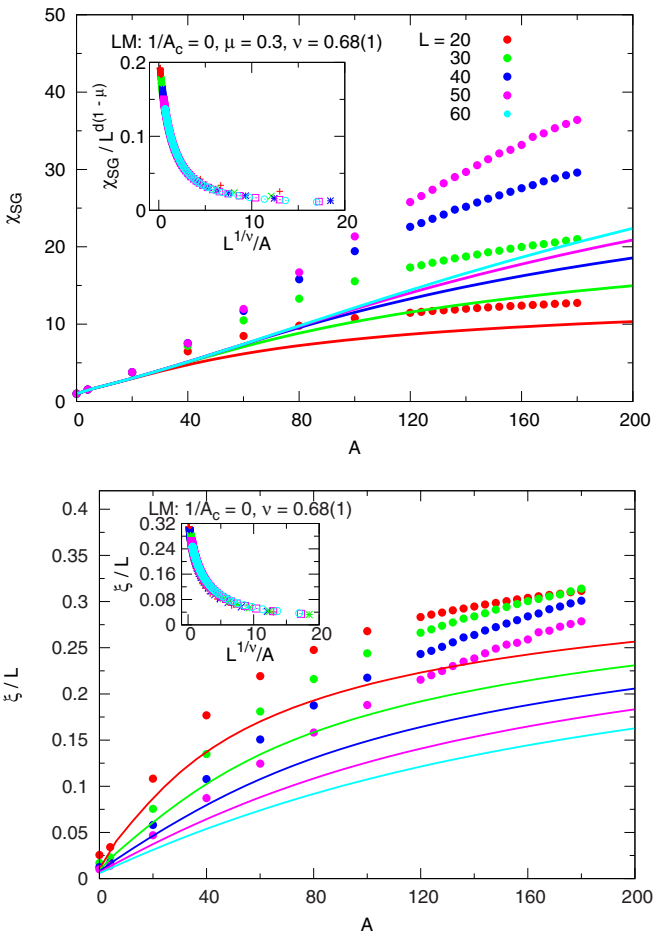

FIG. 3. (Color online) Spin glass susceptibility (top) and correlation length (bottom) for the LGF interaction. Several system sizes are indicated by different colors. Circles represent MC simulations (error bars are of the order of the circle size), and lines are from the LM approach—correlations are stronger for Heisenberg spins than the "soft" LM spins throughout. Insets: Scaling collapse for LM for $1/A_c = 0$.

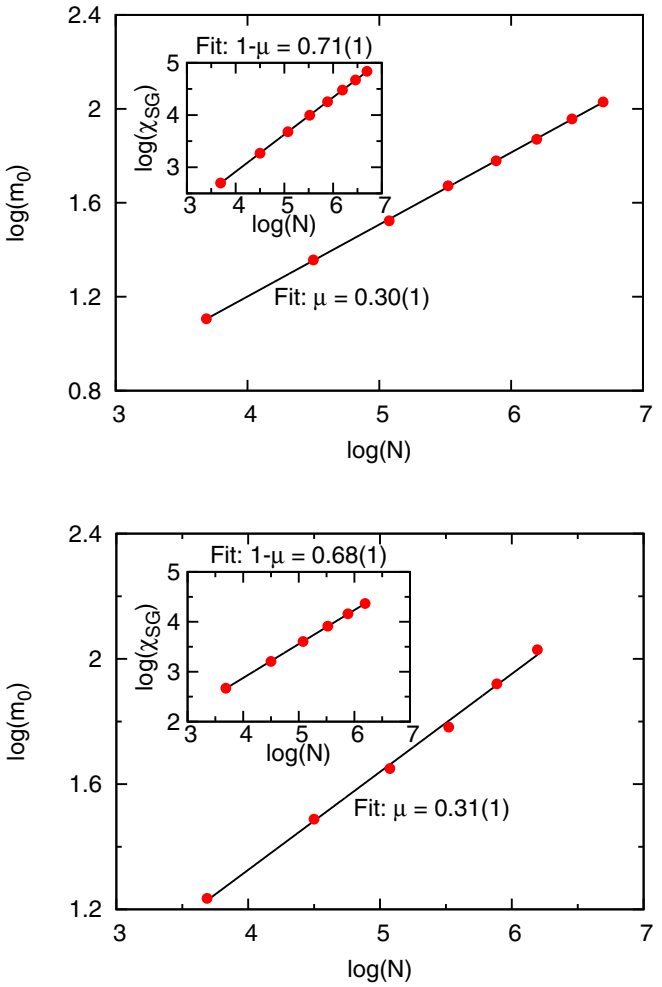

FIG. 4. (Color online) Scaling of the number of zero eigenvalues (m_0) of matrix B defined in the text and of the spin glass susceptibility (insets) with the number of particles for the LGF (top) and log (bottom) interactions.

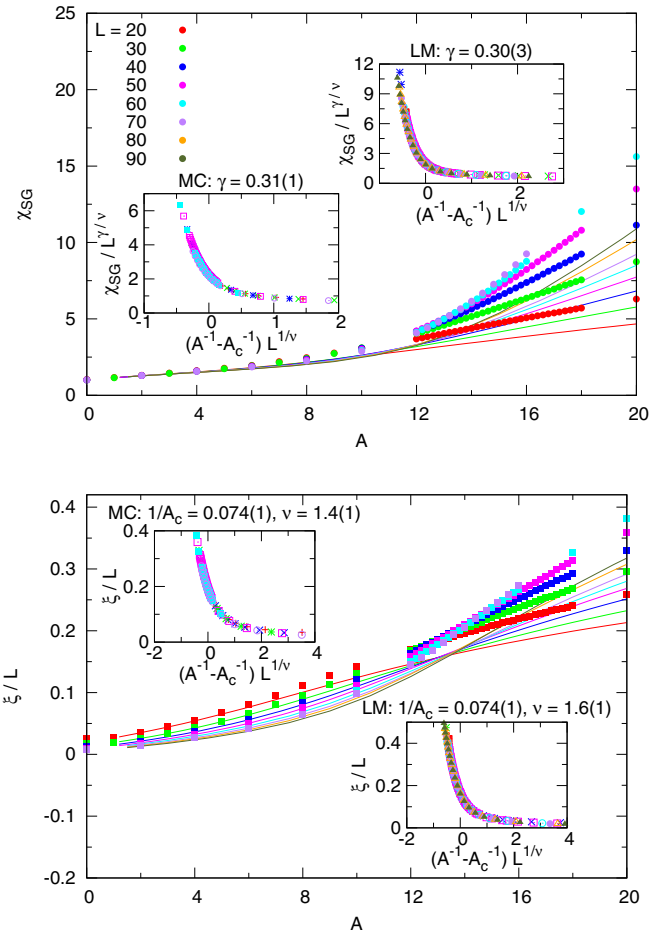

FIG. 5. (Color online) Spin glass susceptibility (top) and correlation length (bottom) for the log interaction, as computed in the MC simulations (points) or with the LM approach (lines). Insets: The corresponding scaling collapses.

Globally, correlations are stronger for the MC simulations on Heisenberg spins compared to the LM results. This is in keeping with the general lore that a lower number of spin components is conducive to spin freezing, as is well known from the comparison of Ising and Heisenberg spins.

In the broad range of coupling strengths considered by our analysis, no unique crossing for the different system sizes of the correlation length curves can be identified.

The LM analysis at $A = \infty$ yields the exponent μ as indicated in Fig. 4. This seems to have the same value, $\mu \approx 0.3$, for both the LGF and the log interactions. The exponent value $\mu = 0.3$ is used as input, together with the assumption that $A_c = \infty$ for the LGF, in attempting a scaling collapse of the LM data. The exponent ν was determined by a fitting procedure with the scaling relation, Eq. (30), *only using data for the correlation length*. The resulting scaling collapse is shown in the inset in the bottom panel in Fig. 3, where $\nu = 0.68(1)$ is obtained. Finally, we use all these exponents in the predicted scaling relation for the susceptibility (the result is shown in the inset in the top panel in Fig. 3). The available data from the LM calculations therefore indicate a freezing transition at $A_c = \infty$ for the diluted model with the LGF as the interaction in two dimensions.

The log interaction turns out to lead to a dramatically different behavior! This is a surprising result, as the interactions differ appreciably only at large distances (Fig. 2). Figure 5 shows the results for the observables of interest as obtained from MC simulations and LM calculations, respectively. Here again we fix the density of particles $x = 0.1$ and consider 200 disorder realisations. A clear crossing of the correlation length curves for different system sizes occurs and scaling collapses of the data are possible, which are shown together with the corresponding critical exponents in the insets.

To study this effect more closely, we consider the pair correlations as a function of the relative coordinates of the pairs, averaged over disorder realizations (Fig. 6). The profile is isotropic for the LGF, with only the first few nearest neighbors significantly antiferromagnetically correlated. On the other hand, the log interaction yields strongly anisotropic behavior (the interaction itself is anisotropic) and this seems to be responsible for what we see as a "glassy phase transition" emerging from the "splaying-out" of the susceptibility curves. The absence of glassiness is explained in more detail in Appendix A, where we expose how the pair correlation profile

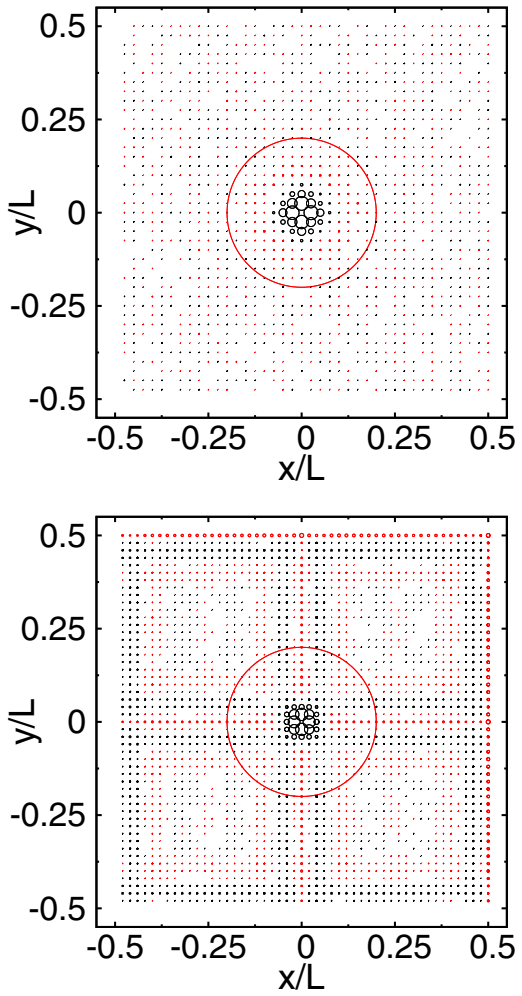

FIG. 6. (Color online) Disorder-averaged pair correlations with a spin at the origin as a function of the relative coordinates. The center of each circle indicates the position of the spin, and its radius gives the magnitude, with red (black) denoting positive (negative) correlations. The large central (red) circle thus reflects $\langle \vec{S}_i^2 \rangle = 1$. Top: Result for the LGF with $A = 100$. Bottom: Result for the log with $A = 20$. MC data are in agreement with LM data (not shown).

helps us to define an appropriate susceptibility for the case at hand, which is shown to diverge in the thermodynamic limit. It turns out that this reflects not the existence of true glassiness but a transition closer to conventional ordering. Note that the gross features of the correlations (Fig. 6, bottom) follow if one frustrates the pairs at the kink (Fig. 2) of the log interaction, which form a frame at half the system size. The set of points which in turn are in the "frames" of $O(L)$ points in the first frame yields the cross-shaped set of ferromagnetically correlated sites centered on the origin.

Note that such finite-size differences appear to be absent in previous studies in $d = 1$ [29]; they appear to be a consequence of the anisotropic nature of our periodized log interaction with its nonanalytic minimum at maximum separation. By contrast, the "smoothed log" (Fig. 2) that also respects the periodic boundary conditions essentially reproduces the LGF interaction results.

1. The fully covered square lattice

For completeness, we have also analyzed the situation for a fully occupied lattice. In this case we observe that the LGF interaction leads to conventional (Néel) antiferromagnetic order, while the log leads to a "striped" phase. This can be understood from a theorem in Ref. [30] which states that the ground state of the system is determined by the minimum of the Fourier transform of the interaction. This is explained in more detail in Appendix B.

B. Three dimensions

We analyze the diluted cubic lattice considering a density of particles $x = 0.0625$, and again considering the model Hamiltonian of Eq. (1), with interactions now restricted to be the LGF as given by Eq. (16). Both MC simulations and LM calculations cover several system sizes, with 100 distinct disorder realizations each. The main focus is on the possibility of a glassy phase, and the spin-glass susceptibility and corresponding correlation length are computed. Our prior discussion of the finite-size scaling relations still holds, and one determines the transition as a unique crossing of the finite-size correlation length curves. Instead of this we observe (Fig. 7) a trend for the crossings to shift towards larger values of A

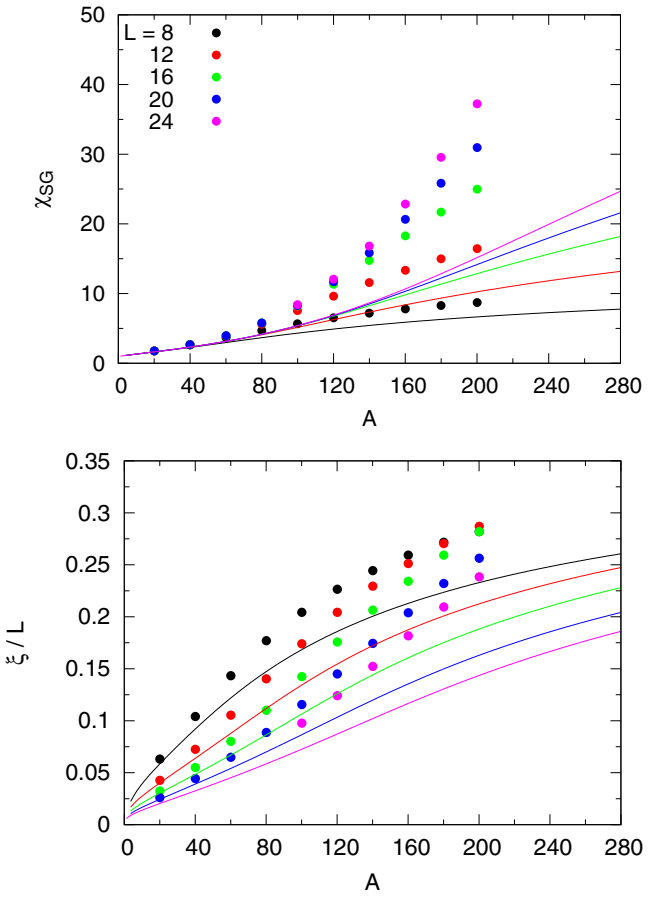

FIG. 7. (Color online) Spin-glass susceptibility (top) and correlation length (bottom) computed from the LM approach (lines) or measured in MC simulations (points), for the LGF interaction on a cubic lattice.

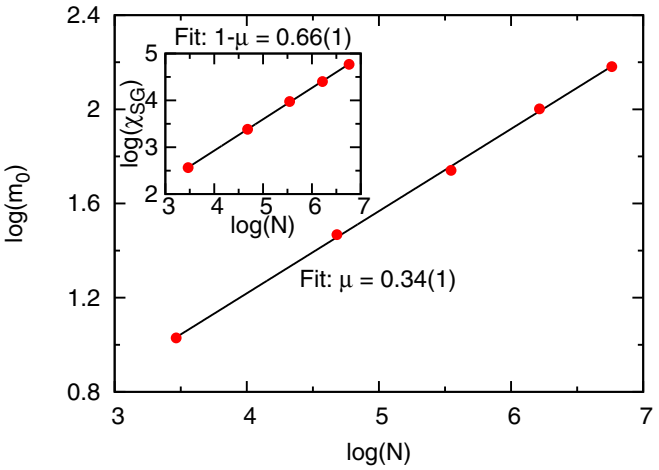

FIG. 8. (Color online) Scaling of the number of vanishing eigenvalues of matrix B defined in the text and of the spin glass susceptibility (inset) with the number of particles for the LGF in three dimensions at $1/A = 0$.

as the system size increases, similar to the situation in two dimensions.

No good scaling collapse was obtained. A freezing transition in this system at a finite coupling strength therefore appears unlikely, though a more careful finite-size scaling analysis of the crossings is necessary to give a definitive answer.

An LM study at $A = \infty$ reveals that the exponent for the scaling of zero eigenvalues of matrix B with the system size yields $\mu = 0.33$ (Fig. 8), in agreement with the prediction in three dimensions for a short-ranged-interacting system [25]. Use of this exponent and the scaling relations at $A = \infty$ does not lead to a good scaling collapse of our LM data, reinforcing the conclusion that this system does not present any freezing transition at $A = \infty$.

The pair correlations exhibit the same sort of behavior as in the $d = 2$ case: only the first few nearest neighbors tend to be strongly antiferromagnetically correlated, and no correlations develop at large distances as the coupling strength is increased, so the system remains paramagnetic.

V. SPECTRAL PROPERTIES

The $A^{-1} = 0$ transition can be considered from the point of view of the interaction matrix J_{ij}, (16) and (17), as an example of an ERM [18]: Unlike the traditional random matrices, where different entries in the matrix are uncorrelated, ERMs are defined as a function of the distance between two points $f(r)$, where the randomness in the entries is induced by the randomness of the underlying point pattern $\{\mathbf{r}_i\}$. These random matrices have been studied for certain classes of functions f [19], and some classical results are available. Our degree of understanding of this subject is not comparable to that of the classical ensembles (e.g., GOE, GUE, Wishart) [31], with most results coming from exact diagonalization and approximations [18,19,32].

Unfortunately due to the long-range nature of the log interaction, many of the methods for analyzing the spectral properties presented in Ref. [19] do not apply directly to our case. However, a phenomenological picture of the low- and high-lying eigenstates of the matrix J_{ij} can be established transparently.

Let us start from the large positive eigenvalues. Since J_{ij} is constant in sign, the Frobenius-Perron theorem states that the highest eigenvector is nodeless. To a reasonable approximation, it is fully delocalized:

$$\phi^{(N)} \simeq (1/\sqrt{N}, \ldots, 1/\sqrt{N}). \tag{31}$$

The associated eigenvalue is

$$\lambda_{\max} \sim \frac{N}{2} \ln N, \tag{32}$$

with an inverse participation ratio (IPR) of $1/N$.

The second-to-highest eigenvalue is also associated with a delocalized eigenvector, which is now a wave with wavelength $\lesssim L$. At these length scales the randomness of the point process plays little role. A finite fraction (possibly all) of the eigenstates containing the largest eigenvalues is *delocalized*, they correspond to long-wavelength charge-density variations. The average spectral density (DOS) of the LGF, (16), interaction matrices is shown in Figs. 10 and 11 (top), in the limits of high ($x = 0.125$) and low density ("continuum limit"; $x = 2^{-13}$), respectively.

Guided by the numerics, we see that the eigenvectors corresponding to the most *negative* eigenvalues are localized: most of the weight is concentrated in $O(1)$ spins. This leads us to consider isolated percolation animals.

The simplest (and, for small x, the most abundant) of these is the dimer. A well-isolated dimer supports two eigenvalues: an antisymmetric and a symmetric one. The antisymmetric one,

$$\phi^{(0)} = (1/\sqrt{2}, -1/\sqrt{2}, 0, \ldots, 0), \tag{33}$$

corresponds to the smallest eigenvalue. In fact, since the closest pair is located one lattice spacing away, $J_{12} \sim \ln L$ and the lowest eigenvalue is

$$\lambda_{\min} \simeq -\ln(L) + O(1) \simeq \tfrac{1}{2}\ln(N/L^2) - \tfrac{1}{2}\ln(N) + O(1). \tag{34}$$

At a fixed density, N/L^2, the lowest eigenvalue depends logarithmically on the system size.

For a well-isolated dimer, say, at distance r from the closest spin, the effect of neglecting the rest of the spins appears as a correction $O(1/r)$. We now consider how large this isolation distance r is. By the usual arguments of percolation theory, one can estimate the expected number of isolated dimers as

$$n_d(r) = L^2 2x^2(1-x)^{\pi r^2}, \tag{35}$$

where we have approximated the number of lattice sites in a circle of size r with πr^2. Therefore the most isolated dimer [the solution of the equation $n_d(r) = 1$] is surrounded by an empty area of size

$$r(L) = \frac{\sqrt{2\ln(xL\sqrt{2})}}{\sqrt{\pi \ln(1/(1-x))}}. \tag{36}$$

Note the extremely slow dependence $r(L) \sim \sqrt{\ln L}$.

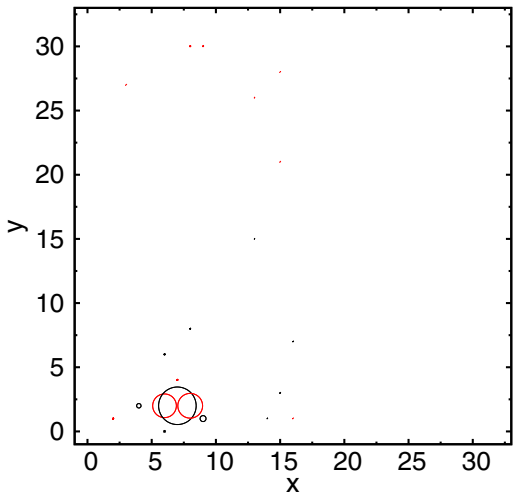

FIG. 9. (Color online) Ground-state eigenvector showing a trimer for a particular disorder realization using the LGF as the interaction on a lattice of size $L = 32$ with $N = 102$ particles. The components of the eigenvector are proportional to the radii of the circles, which are centered on the corresponding spin position. A red (black) circle indicates a positive (negative) sign.

Inserting $L = 120$ and $x = 0.1$, which are about the largest sizes considered in our numerics, $r = 4.13$, which can hardly be called isolated. The isolation effect would be much more pronounced for $x = 10^{-3}, L = 1{,}200$, for which $r = 18.4$. Otherwise, one needs to consider the ground states of more complicated lattice animals, like trimers, snakes, squares, etc. As an example, a ground-state eigenvector for one disorder realization is shown in Fig. 9.

This problem becomes quickly analytically prohibitive. However, the fact that the ground state is localized on some lattice animal appears robust: in the graphs we consider, the smallest eigenvalue is $\sim -\ln L$ and the IPR is $O(1)$.

With the lower end of the spectrum localized and the high-end delocalized, it is a natural question whether there exists a mobility edge separating the two limits. In order to study the transition we have looked at the IPR as a function of the eigenvalue λ:

$$\begin{aligned} \mathrm{IPR}_\alpha &= \sum_i v_{\alpha i}^4, \\ Y(\lambda) &= \frac{1}{\rho(\lambda)} \sum_\alpha \mathrm{IPR}_\alpha \delta(\lambda - \lambda_\alpha), \end{aligned} \tag{37}$$

where λ_α and $v_{\alpha i}$ are eigenvalues and normalized eigenvectors of J_{ij}, respectively. We consider the average $[Y](\lambda)$ and fluctuations $\sigma(Y)(\lambda)$ [33]. A mobility edge would be signaled by the divergence of the fluctuations of $Y(\lambda)$ at a certain λ_c. Numerical diagonalization of J_{ij} does not indicate such a transition: the two limits appear to be separated by a crossover. The bottom panels in Figs. 10 and 11 show, respectively, for a high and low density of particles, the average $Y(\lambda)$, while the insets display the fluctuations of $Y(\lambda)$. The spectral properties of the LGF in $d = 3$ turn out to be very similar to those in the $d = 2$ case (not shown).

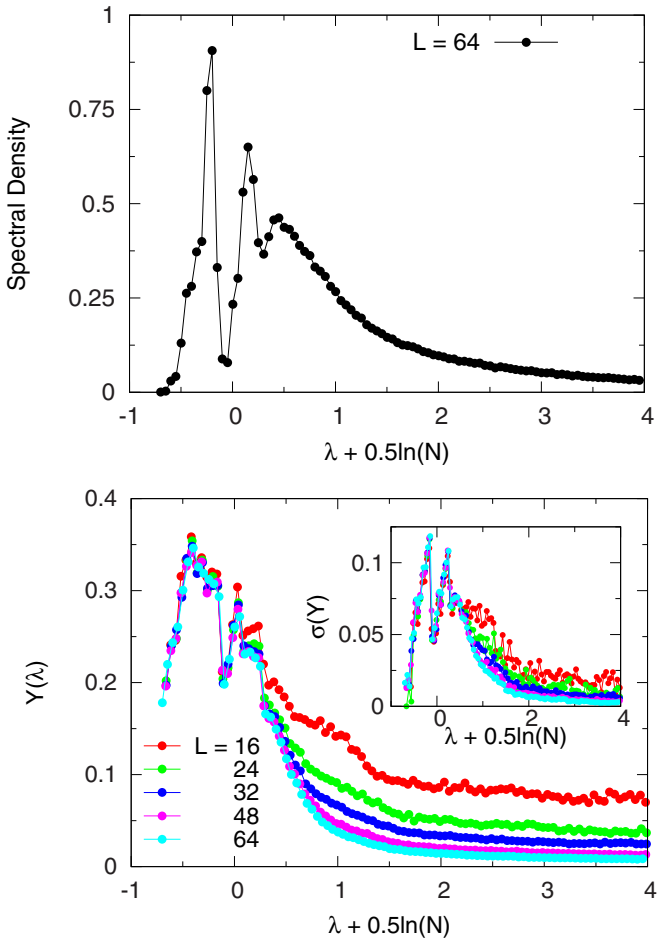

FIG. 10. (Color online) Spectral density (top) and average Y (Eq. 37, bottom) for a fraction of $x = 0.125$ occupied sites in the lattice, using J_{ij} as defined in (16), the LGF interaction. The inset shows the fluctuations of Y.

A detailed study of this ERM ensemble would be desirable and is left for future work.

VI. PAIR CORRELATIONS AND SCREENING

A. Analytical theory of screening

Away from the $T \to 0$ limit of the microscopic model, excitations of the nonorphan tetrahedra out of their momentless state carry a gauge charge, which leads to a variant of Debye screening, with the special feature that the gaplessness of the charge excitations leads to a somewhat unusual temperature dependence of the screening length [34].

In addition to this, even in the limit $T \to 0$ studied here, we encounter an additional type of screening. This occurs on account of the long-range uniformly antiferromagnetic Coulomb interaction between the orphans, whose existence is the distinguishing property of the random Coulomb antiferromagnet. It again exhibits a Debye form, although distinct from the setting of mobile charges in which Debye screening is normally considered, as here it is the (continuous) flavor of the charges—the orientation of the orphan, whose orientation is free but whose location is fixed—which is the dynamical degree of freedom.

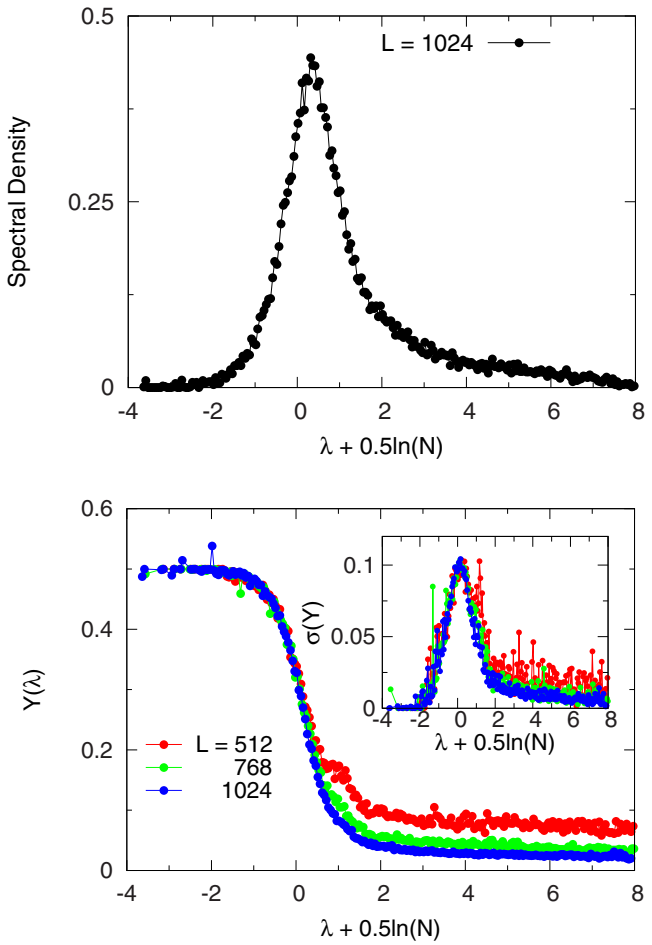

FIG. 11. (Color online) Spectral density (top) and average Y (bottom) for a fraction of $x = 2^{-13}$ occupied sites in the lattice, using J_{ij} as defined in (16), the LGF interaction. Inset: Fluctuations of Y.

This can be seen directly in a weak-coupling expansion, which in Coulomb systems has a vanishing radius of convergence in the thermodynamic limit, as is easily verified in our simulations (Fig. 12).

To elucidate the role of screening, we compute the disorder-averaged correlator between two spins at r_a and r_b. Consider the Hamiltonian

$$H = \frac{\alpha}{2}\sum_{i,j} J_{ij}\vec{n}_i \cdot \vec{n}_j, \tag{38}$$

where J_{ij} are given by either the log or the LGF and we eventually set $\alpha = 1$. The correlation function between two spins, for fixed disorder, is (Fig. 13)

$$C_{ab} = \langle \vec{n}_a \cdot \vec{n}_b \rangle = \frac{1}{Z}\int d^{3N}n \prod_i \delta\left(1-n_i^2\right)(\vec{n}_a \cdot \vec{n}_b) e^{-\frac{\alpha}{2}\sum_{i,j} J_{ij}\vec{n}_i\cdot\vec{n}_j}. \tag{39}$$

As it is not the hard-spin constraint which is central to the physics of screening, we substitute it with something more manageable (analogously to the LM method, but without imposing self-consistency). Representing the δ function with

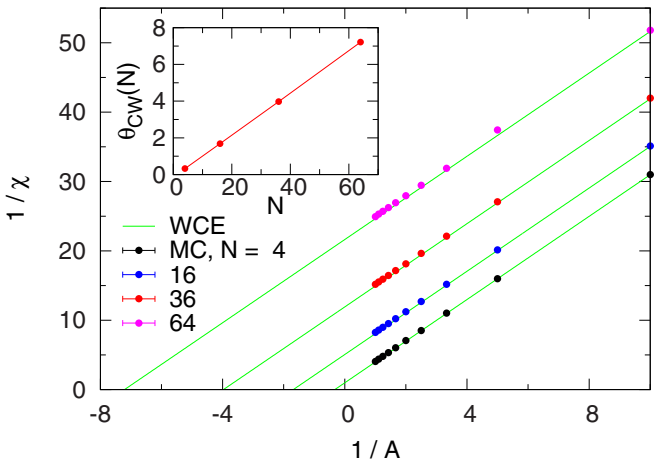

FIG. 12. (Color online) Uniform susceptibility as computed from MC simulations (points) compared to a weak-coupling expansion (WCE) averaged over 200 disorder realizations (dashed lines). The Curie-Weiss constant increases approximately linearly with the number of particles (inset), yielding a vanishing radius of convergence of the weak-coupling expansion already at leading order.

a Gaussian term,

$$\delta\left(1-n_i^2\right) \to \frac{1}{(2\pi/3)^{3/2}} e^{-3\frac{n_i^2}{2}} \tag{40}$$

(with a factor of 3 to guarantee that $\langle n_i^{x2} + n_i^{y2} + n_i^{z2}\rangle = 3/3 = 1$). Thus

$$C_{ab} = \delta_{ab} - \langle a| \frac{\frac{1}{3}\alpha J}{1+\frac{1}{3}\alpha J} |b\rangle, \tag{41}$$

where we use the matrix notation $\langle a|J|b\rangle = J_{ab}$. For simplicity we do not write the δ_{ab} term, which only affects the result for the self-correlation (it will again be important when we discuss the LM approximation later). The correlation function between a and b depends also on the positions of all the other points $x_2, \ldots, x_N$ so it should be written as $C(x_a, x_b|x_2, \ldots, x_N)$.

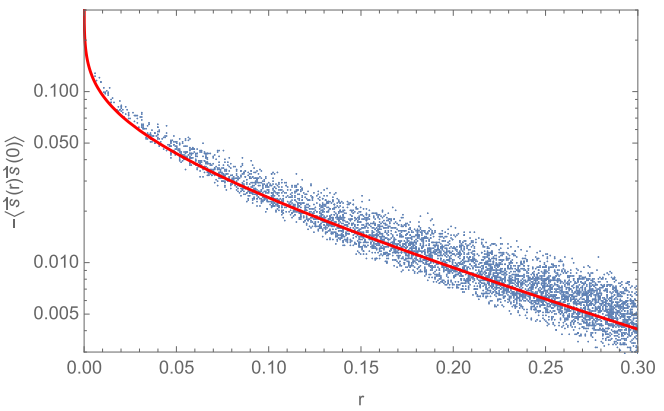

FIG. 13. (Color online) Correlation function exhibiting screening: numerical results (for a single disorder realization with $N = 200$ points on a square of unit size) compared to the analytical form predicted from the chain diagrams.

This Gaussian approximation is equivalent to the resummation of a set of diagrams in which there are no internal loops, dubbed "chain diagrams." This approximation is justified in the limit of small α, in which spins are rarely polarized along some direction and the hard-spin constraint is not as important.

This result holds for each disorder realization. We now take the average over realizations (leaving the question whether or not this is representative of the distribution for later), keeping fixed the position of the two spins a and b. To do this, it is convenient to go back to the geometric expansions and define

$$\mathbf{E}[C_{ab}] \equiv \int \frac{d^{N-2}x}{S^{N-2}} C(x_a, x_b | x_1, \ldots, x_{N-2}), \tag{42}$$

where x_i are the locations of the other $N-2$ spins and $S = L^2$. We have relaxed the constraint that points be located on a square lattice, which is immaterial in our high-temperature, low-dilution expansion.

Unfortunately it is difficult to see what the distribution of J induced by the random positions is, but we can expand the Gaussian result in powers of α and do the average term by term. We get

$$\mathbf{E}[C_{ab}] = -\frac{1}{3}\alpha J_{ab} + \sum_i \left(\frac{1}{3}\alpha\right)^2 \mathbf{E}[J_{ai} J_{ib}] - \left(\frac{1}{3}\alpha\right)^3 \sum_{ij} \mathbf{E}[J_{ai} J_{ij} J_{jb}] + \ldots. \tag{43}$$

Now, term by term we obtain objects like

$$\mathbf{E}\left[\sum_i J_{ai} J_{ib}\right] = (N-2) \int \frac{d^2x}{S} J(x_a - x) J(x - x_b) = \rho \int d^2x\, J(x_a - x) J(x - x_b), \tag{44}$$

where $\rho = (N-2)/S \simeq N/S$ is the density of points. Fourier transforming,

$$\rho \int d^2x\, J(x_a - x) J(x - x_b) = \rho \int d^2x \frac{d^2q}{(2\pi)^2} \frac{d^2q'}{(2\pi)^2} J_q J_{q'} e^{iq(x_a - x) + iq'(x - x_b)} \tag{45}$$

$$= \rho \int \frac{d^2q}{(2\pi)^2} J_q^2 e^{iq(x_a - x_b)}. \tag{46}$$

The geometric series thus obtained for $\mathbf{E}[C_{ab}]$ yields

$$\mathbf{E}[C_{ab}] = -\int \frac{d^2q}{(2\pi)^2} e^{iq(x_a - x_b)} \frac{(\alpha/3) J_q}{1 + (\alpha\rho/3) J_q}. \tag{47}$$

Now, for both the log and the LGF, $J_q \simeq c/q^2$ [c is a constant of $O(1)$] [35], so that at small α we have approximately

$$\mathbf{E}[C_{ab}] \simeq -\int \frac{d^2q}{(2\pi)^2} e^{iq(x_a - x_b)} \frac{(c\alpha/3)}{q^2 + (c\alpha\rho/3)}. \tag{48}$$

This leads to

$$\mathbf{E}[C_{ab}] \simeq (-2\alpha/3) K_0(r\sqrt{c\alpha\rho/3}), \tag{49}$$

which exhibits a screening length

$$\xi = 1/\sqrt{c\alpha\rho/3}. \tag{50}$$

As both α and c are $O(1)$, this shows (not surprisingly) that the screening length is proportional to $1/\sqrt{\rho}$.

Note that in this approximation, for $r_{a,b} \ll \xi$ the correlation function $C(r) \gg 1$, which is not physical for unit length spins. This is an artifact resulting from substituting a quadratic confining potential for the hard-spin constraint. Therefore this approximation is internally consistent only for $r_{a,b} \gtrsim \xi$, where it predicts an exponential damping of the correlations, but we note that the large *anti*correlations at short distances, due to strongly coupled spins close to one another, put these into a state with vanishing total spin, which—physically correctly—screens their joint field at larger distances.

B. A random scattering picture

The final question we address concerns the fluctuations of the random quantity, (41), and whether these may signal any phase transition even when the mean does not. To gain some insight into this, we develop an analogy with wave propagation in disordered media, which suggests that no transition exists. The basic observation is that the interaction is simply related to the inverse of the Laplacian, the propagator of a free particle on the lattice:

Considering that

$$J_{ij} = \langle i | \frac{1}{-\nabla^2} | j \rangle \tag{51}$$

properly regularized (particularly important is the condition that $J_{ii} = 0$), we can rewrite expression (41) as

$$C_{ab} = \delta_{ab} - \frac{\alpha}{3} \langle a | \frac{1}{-\nabla^2 + V - E} | b \rangle, \tag{52}$$

where $E = 0$ and

$$V(x) = \frac{\alpha}{3} \sum_i \delta(x - x_i) \tag{53}$$

is a random potential. This can be established by expanding in powers of α. Thus C is (proportional to) the propagator for a wave in a two-dimensional box with randomly placed pointlike scatterers [36,37], at energy $E = 0$.

The precise form of the mapping is the following: The correlation function,

$$-\frac{1}{\alpha} C_{ab} = -\frac{3}{\alpha} \langle n_a n_b \rangle, \tag{54}$$

is the amplitude of a signal sent from the scatterer a to the scatterer b, considering all order processes bouncing over all the N scatterers. In the case where $a = b$ the direct path from a to b needs to be neglected. This is a form of *renormalization* of the scattering problem, which is always necessary in the pointlike (or s-wave) scattering limit [38].

Once the renormalization procedure is done, the problem we are left with corresponds to the propagation of a scalar wave, damped by a scattering section for every typical realization of disorder. Without repeating the classical treatment of this phenomenon we can say that the signals (spin-spin correlations) must be screened for any α, the screening length (measured in units of $1/\sqrt{\rho}$) being a decreasing function of α. Even if not precisely of the form (50) for small α, it seems to diverge like $1/\sqrt{\alpha}$.

This is valid for both the *coherent* field $\mathbf{E}[C_{ab}]$ and the *incoherent* field $\mathbf{E}[C_{ab}^2] - \mathbf{E}[C_{ab}]^2$, although the scattering sections (and hence the damping/correlation lengths) might have different values. This analogy makes us realize that in this approximation there is *no transition*, irrespective of the value of α or ρ, and this is consistent with numerical results.

This analogy extends also to the LM limit. Considering a small-α series expansion for the spin correlation function,

$$h_a C_{ab} h_b = \delta_{ab} h_a - \alpha J_{ab} + \alpha^2 J_{ai} \frac{1}{h_i} J_{ib} - \alpha^3 J_{ai} \frac{1}{h_i} J_{ij} \frac{1}{h_j} J_{jb} + \dots \quad (55)$$

(recall that in the LM approach α is scaled by a factor $1/m$, hence the factor of 3 in the previous paragraphs is absent here), where the extra factors of h_a need to be chosen in such a way that

$$C_{ii} = \langle n_i n_i \rangle = 1. \quad (56)$$

C_{ab} is then proportional to the propagator

$$G_{ab} = \tilde{h}_{ab} - \alpha \langle a | \frac{1}{-\nabla^2 + V - E} | b \rangle, \quad (57)$$

where $\tilde{h}$ is the diagonal matrix with diagonal entries $\{h_i\}_{i=1,\dots,N}$, $E = 0$, and

$$V(x) = \alpha \sum_i \frac{1}{h_i} \delta(x - x_i), \quad (58)$$

where the renormalized value $\langle i | \frac{1}{-\nabla^2} | i \rangle = 0$ is intended.

This is a scattering problem over pointlike scatterers, where now each scatterer has a different scattering amplitude. This modification should not change the physical analogy of the problem. This is again a scattering problem of a scalar wave over pointlike scatterers. The propagation of the wave is attenuated over distance in the usual exponential fashion. Therefore, if a phase transition exists, it is not mirrored in the divergence of the correlation length. Conversely, as this treatment is closely related to the LM one (rather than the Heisenberg model), on account of the softening of the hard constraint to a Gaussian one, we would not expect a transition at a finite value of α.

VII. DISCUSSION

We have studied the effective theory describing disorder in the form of quenched nonmagnetic impurities, in the topological Coulomb phase, on a lattice with a bipartite dual lattice. Interactions in the effective picture are long-ranged, and to the best of our knowledge, this is the first study available of such a model.

A. A freezing transition?

Our results show that any freezing transition, if it exists, is extremely tenuous. In $d = 2$, for LM there does not appear to be freezing for any finite coupling, with a nice scaling collapse of the data at $A = \infty$, indicating freezing to take place in this limit.

The relation of this result to a finite number of spin components is the following. First, our Heisenberg simulations cannot access a freezing transition, but they do show a greater tendency towards glassiness than the LM data, with both a larger spin-glass correlation length and an enhanced tendency for the curves to cross.

This is in keeping with the general expectation [25] for the more constrained Heisenberg model to freeze before the soft spins do (and after an Ising model might). If there is a freezing transition at $A_c < \infty$, it will still be at the fantastically large coupling $A_c > 100$. The delicate nature of all of these phenomena is further underscored by the dependence on finite-size choices, which may lead to an entirely different set of instabilities. Similarly, the analytical approaches, in particular, the mapping to a quantum scattering problem, show little indication of a transition.

The tendency towards freezing seems to be even weaker in $d = 3$, perhaps surprisingly so, given that the freezing transition is more robust in higher dimensions for instances of canonical spin glasses. However, unlike in these cases, our distribution of the intersite couplings is dimensionality dependent and, in particular, becomes "shorter-ranged" as the power law of the decay of the Coulomb law grows with d (while, of course, the power law with which the number of distant spins grows increases).

The weak tendency towards freezing is in keeping with the fact that our model is not easily deformed into one of the standard spin-glass models. On one hand, increasing the range of the interaction towards the extreme of doing away with any notion of distance and assigning equal coupling between all the spins yields simply a global charge-neutrality constraint (which, at any rate, is already enforced microscopically) and therefore preserves a microcanonical version of a *perfect paramagnet*. If the coupling is restricted to nearest neighbor, we instead get a combination of percolation physics and that of the standard Néel state for a bipartite antiferromagnet, where any tendency towards disorder is a dimensionality effect, and glassiness is nowhere to be seen.

The tendency towards glassiness is therefore necessarily due to a combination of the nonconstancy of the logarithmic interaction—which, helpfully, is not bounded as $r \to \infty$—along with its long range. Studying models exhibiting this pair of ingredients more systematically is surely an interesting avenue for future research. We would like to emphasize, in particular, that the phenomenon of screening we have discussed has no counterpart in the literature on conventional spin glasses, where random choice of the sign of the interactions does not allow the identification of an underlying charge structure.

In this sense, our model is much closer to those familiar from the study of Coulomb glasses, although the differences here are again considerable. We have vector charges rather than Ising (positive or negative) ones; disorder appears in the form of random but fixed *locations* rather than fixed on-site potentials for charges not bound to a particular site. It is intriguing that such a variation of a classic Coulomb glass appears entirely naturally in frustrated magnetism.

B. Freezing in frustrated magnetic materials

With Heisenberg spins placed at random sites of a pyrochlore-slab lattice (also known as an SCGO lattice) and a

particular, microscopically determined value of A, the $d = 2$ case of our Coulomb antiferromagnet corresponds, up to the sublattice-dependent inversion factor mentioned earlier, to the $T \to 0$ limit of the physics of orphans created when a pair of Ga impurities substitutes for two of the three Cr spins in a triangular simplex of this lattice. Although experimental interest in SCGO dates back to the 1980s and played a key role in stimulating experimental and theoretical interest in the area of highly frustrated magnetism [11], the behavior of SCGO is reasonably well understood in theoretical terms only in the broad Coulomb spin-liquid regime down to about a hundredth of the exchange energy scale (of order 500 K) between Cr spins. The magnetic response in this regime can be modeled in a rather detailed way as being made up as the response of a pure Coulomb spin liquid superposed with the Curie tails associated with vacancy-induced "orphan" degrees of freedom [5–8], which carry an effective fractional spin [4,10] and leave their imprint on NMR lineshapes [10] and bulk susceptibility [5,6,10] in the Coulomb spin-liquid phase. In contrast, the physics at very low temperatures (of order 5 K or lower) is still not very well understood, with intriguing but largely unexplained reports of observed glassy behavior even at very low densities of Ga impurities [12,15], which appears to involve only the freezing of a fraction of its degrees of freedom.

Our model retains the key feature of the $T \to 0$ limit of the effective model, namely, the long-range Coulomb form of the effective exchange couplings, but does not retain the detailed geometry of these orphans in SCGO, except for the sublattice-dependent inversion that connects the degrees of freedom of our Coulomb antiferromagnet with the underlying physics of these orphans.

Bearing all this in mind, the usual caveat about idealized models for frustrated systems applies to our study as well: Our starting Hamiltonian of a classical nearest-neighbor Heisenberg model does not include a number of aspects—farther-neighbor interactions, single-ion anisotropies, noncommutation of spin components—all of which give rise to interesting, generally nonglassy, physics of their own. If and when these energy scales dominate over our the instabilities of the idealized model, it is the former which will likely show up more prominently in experiments.

In addition, in our case, the critical coupling A_c, even if it is not infinite, is hard to attain in any microscopic model. Indeed, for a checkerboard lattice, one obtains $A = 1/4\pi$ from a microscopic calculation, easily within a very short-range correlated regime.

At any finite temperature, which is all that can be accessed experimentally for the time being, Coulomb interactions obtain a finite-screening length due to the thermal excitation of charges even in nonorphan tetrahedra. Following the general lore on spin freezing, this precludes even canonical Heisenberg spin glassiness. For this reason, the above-mentioned A independence of a freezing transition in $d = 2$ is not going to carry over directly to the experimental compound.

However, real systems will only be quasi-two-dimensional, with residual couplings between the two-dimensional layers. Indeed, for the case of SCGO, dilution also breaks up the tightly bound singlets of the dimers of Cr ions which isolate the kagome-triangle-kagome trilayers from one another. The consequences of coupling in the third dimension remain an interesting yet completely open topic for future study.

C. Connection to other models

More broadly, perhaps the most pleasing aspect of this work is how it naturally connects (with) a number of deformations of well-known problems: the scattering problem, Coulomb glass physics, and random matrix theory. In particular, we have identified a straightforward way of obtaining an ERM problem from a simple magnetic model where long-range interactions emerge naturally. We hope that this will motivate further work on any (and perhaps all) of these problems.

ACKNOWLEDGMENTS

We are very grateful to John Chalker, Ferdinand Evers, Mike Moore, and Peter Young for useful discussions. This work was supported by DFG Grant No. SFB 1143.

APPENDIX A: NONGLASSINESS FOR THE LOG INTERACTION

The pair correlation profiles for the log interaction exhibit a structure hinting at the way pair correlations should be summed in order to define a generalized susceptibility describing the order present in this system. This order reflects the symmetry of the interaction, which is anisotropic but has the symmetries of a square lattice.

We define a *sign function*, $\theta(x,y)$, which, in each quadrant, has alternating values of ± 1 in successive "square frames" of a fixed width of two lattice sites for any L. Assuming (x,y) in the first quadrant, this function has the profile pictured at the left in Fig. 14.

The corresponding susceptibility reads

$$\chi = \left[\frac{1}{N} \sum_{i,j} \theta(\vec{r}_{ij}) \langle \vec{S}_i \cdot \vec{S}_j \rangle \right]. \tag{A1}$$

Square brackets denote, as usual, the disorder average. This susceptibility diverges with the system size, and its scaling

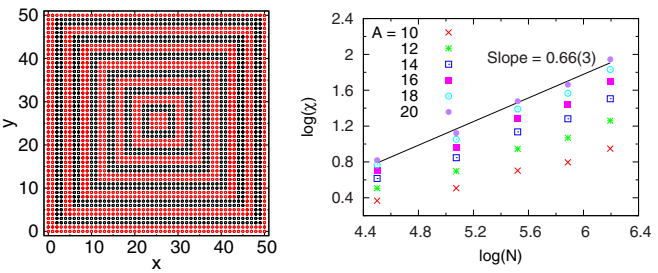

FIG. 14. (Color online) Left: The sign function in the first quadrant for a lattice of side $L = 100$ used to resum the correlations. Right: Scaling of the new susceptibility proposed to describe the ordering occurring with the log interaction.

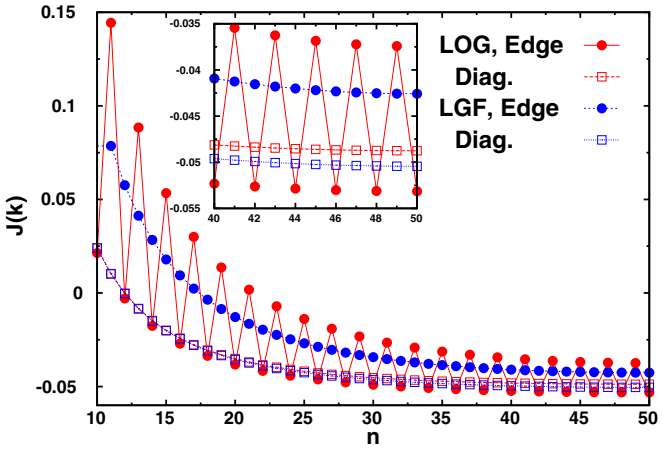

FIG. 15. (Color online) Numerically obtained Fourier transform of the log (red symbols) and LGF (blue symbols) for a lattice of size $L = 100$. Circles connected by lines indicate the edge $k_y = 0$, while squares indicate the diagonal $k_x = k_y$. The index n labeling the x axis indicates the index of the wave vector: $k_x = \frac{2\pi}{L}n$. Inset: The region near the global minimum in more detail.

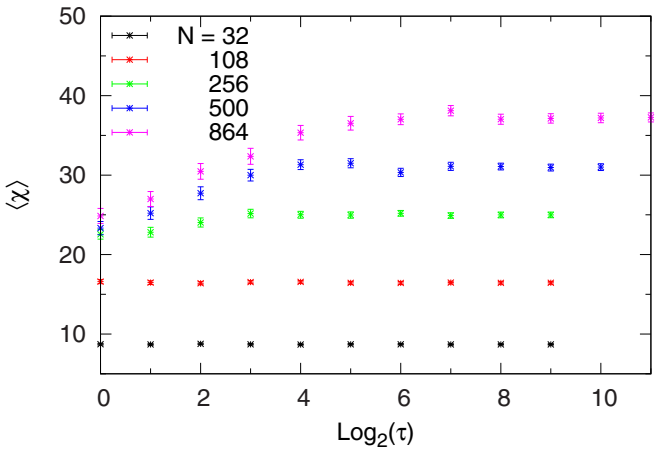

FIG. 16. (Color online) The average in each binning block of the spin glass susceptibilities plotted against the logarithm (base 2) of the size of the corresponding binning block. Data shown here correspond to MC simulation of the LGF in a cubic lattice at $A = 200$.

in MC simulations is shown at the right in Fig. 14; the same behavior is found in the LM data.

APPENDIX B: FULLY OCCUPIED LATTICE

Proposition 1 in Ref. [30] states that if $\hat{J}(k)$ is the Fourier transform of the interaction matrix J, then a minimizer $\vec{k}_0$ for $\hat{J}(k)$ determines a modulated ground state for a system with that wave vector. The Fourier transform of the LGF at nonzero wave vector iseasily read from its definition, Eq. (16),

$$\hat{J}_{\mathrm{LGF}}(k) = \frac{1}{2 - \cos(k_x) - \cos(k_y)}, \tag{B1}$$

which has a minimum at $\vec{k} = (\pi,\pi)$, thence we find "conventional" antiferromagnetic order.

For the log interaction, we are not able to find an analytical expression for its Fourier transform, but numerical results show that the global minima happen at $\vec{k} = (\pi,0)$ or $(0,\pi)$, which explains the striped phase for the fully occupied lattice. The nonanalyticity of the distance function periodized by the function $\min(x,L-x)$ or $\min(y,L-y)$ (which is seen as a discontinuity in the derivative along the lines $x = L/2$ or $y = L/2$) gives rise to "ringing" in $\hat{J}_{\mathrm{Log}}(k)$; a line of alternating local maxima and minima appears along $k_x = 0$ or $k_y = 0$. The new global minimum is shifted from (π,π) to the edges of these lines, as shown in Fig. 15.

APPENDIX C: VERIFYING EQUILIBRATION

Our simulations require exploring a region of very high coupling, A. In this case it is important to ensure that equilibrium is attained. To test this, we bin the data for spin-glass susceptibility. This binning consists of subdividing the total number of measurements, N_m, into contiguous bins of successive sizes: $1, 1, 2, 4, 8, \ldots, N_m/4, N_m/2$. The average for each bin is then plotted against the logarithm of the bin size (Fig. 16). Equilibrium is diagnosed when at least the last three bin averages agree within the interval set by their error bars. The final equilibrium values used consist of the average of the last half of the measurements made in the simulation, $N_m/2$.

[1] R. Moessner and Arthur P. Ramirez, Phys. Today **59**(2), 24 (2006).
[2] L. Balents, Nature **464**, 199 (2010).
[3] K. Binder and A. P. Young, Rev. Mod. Phys. **58**, 801 (1986).
[4] A. Sen, K. Damle, and R. Moessner, Phys. Rev. B **86**, 205134 (2012).
[5] P. Schiffer and I. Daruka, Phys. Rev. B **56**, 13712 (1997).
[6] R. Moessner and A. J. Berlinsky, Phys. Rev. Lett. **83**, 3293 (1999).
[7] C. L. Henley, Can. J. Phys. **79**, 1307 (2001).
[8] C. L. Henley, Annu. Rev. Condens. Matter Phys. **1**, 179 (2010).
[9] D. Sherrington and S. Kirkpatrick, Phys. Rev. Lett. **35**, 1792 (1975).
[10] A. Sen, K. Damle, and R. Moessner, Phys. Rev. Lett. **106**, 127203 (2011).
[11] X. Obradors, A. Labarta, A. Isalgué, J. Tejada, J. Rodriguez, and M. Pernet, Solid State Commun. **65**, 189 (1988).
[12] A. P. Ramirez, G. P. Espinosa, and A. S. Cooper, Phys. Rev. Lett. **64**, 2070 (1990).
[13] B. Martínez, F. Sandiumenge, A. Rouco, A. Labarta, J. Rodríguez-Carvajal, M. Tovar, M. T. Causa, S. Galí, and X. Obradors, Phys. Rev. B **46**, 10786 (1992).

[14] L. Limot, P. Mendels, G. Collin, C. Mondelli, B. Ouladdiaf, H. Mutka, N. Blanchard, and M. Mekata, Phys. Rev. B **65**, 144447 (2002).
[15] A. D. LaForge, S. H. Pulido, R. J. Cava, B. C. Chan, and A. P. Ramirez, Phys. Rev. Lett. **110**, 017203 (2013).
[16] A. Brooks Harris and S. Kirkpatrick, Phys. Rev. B **16**, 542 (1977).
[17] K. H. Höglund and A. W. Sandvik, Phys. Rev. B **70**, 024406 (2004).
[18] M. Mézard, G. Parisi, and A. Zee, Nucl. Phys. B **559**, 689 (1999).
[19] A. Goetschy and S. E. Skipetrov, arXiv:1303.2880.
[20] D. A. Garanin and B. Canals, Phys. Rev. B **59**, 443 (1999).
[21] L. W. Lee and A. P. Young, Phys. Rev. B **76**, 024405 (2007).
[22] J. H. Pixley and A. P. Young, Phys. Rev. B **78**, 014419 (2008).
[23] M. B. Hastings, J. Stat. Phys. **99**, 171 (2000).
[24] T. Aspelmeier and M. A. Moore, Phys. Rev. Lett. **92**, 077201 (2004).
[25] L. W. Lee, A. Dhar, and A. P. Young, Phys. Rev. E **71**, 036146 (2005).
[26] S. V. Isakov, K. Gregor, R. Moessner, and S. L. Sondhi, Phys. Rev. Lett. **93**, 167204 (2004).
[27] F. Beyer, M. Weigel, and M. A. Moore, Phys. Rev. B **86**, 014431 (2012).
[28] L. R. Walker and R. E. Walstedt, Phys. Rev. B **22**, 3816 (1980).
[29] D. Larson, H. G. Katzgraber, M. A. Moore, and A. P. Young, Phys. Rev. B **87**, 024414 (2013).
[30] A. Giuliani, J. L. Lebowitz, and E. H. Lieb, Phys. Rev. B **76**, 184426 (2007).
[31] M. L. Mehta, *Random Matrices*, Vol. 142 (Academic Press, New York, 2004).
[32] A. Amir, Y. Oreg, and Y. Imry, Phys. Rev. Lett. **105**, 070601 (2010).
[33] Numerical evaluation of Y reduces to binning of the eigenvalue interval and computation of the histogram of participation ratios falling into the bins. We define the fluctuations as the sample-to-sample variance of the bin values.
[34] A. Sen, R. Moessner, and S. L. Sondhi, Phys. Rev. Lett. **110**, 107202 (2013).
[35] In order to find the appropriate c we need to specify J. From $c\int \frac{d^2q}{(2\pi)^2}\frac{e^{iqr}}{q^2+2/L} = \frac{c}{2\pi}\ln(\frac{L/\sqrt{2}}{r}) + \text{const.}$, it follows that $J(r) = -\ln(r/L/\sqrt{2})$ implies $c = 2\pi$.
[36] S. Albeverio, F. Gesztesy, R. Høegh-Krohn, and H. Holden (with an appendix by P. Exner), *Wave Propagation and Scattering in Random Media*, Vol. 350.H (AMS Chelsea, Providence, RI, 2005).
[37] A. Ishimaru, *Wave Propagation and Scattering in Random Media*, Vol. 2 (Academic Press, New York, 1991).
[38] A. Scardicchio, Phys. Rev. D **72**, 065004 (2005).